PHILOSOPHICAL TRANSACTIONS OF THE ROYAL SOCIETY A MATHEMATICAL, PHYSICAL & ENGINEERING SCIENCES

Observing the Ocean in the 1990s

W. Munk and C. Wunsch

Phil. Trans. R. Soc. Lond. A 1982 **307**, 439-464
doi: 10.1098/rsta.1982.0120

Phil. Trans. R. Soc. Lond. A **307**, 439–464 (1982)
Printed in Great Britain

Observing the ocean in the 1990s

By W. Munk†, For.Mem.R.S., and C. Wunsch‡
Department of Applied Mathematics and Theoretical Physics, University of Cambridge, Silver Street, Cambridge CB3 9EW, U.K.

To understand the ocean, its dynamics, its role in climate, weather and other ocean–atmosphere phenomena, one must observe it on a basin-wide scale with adequate time and space resolution. No such observation system yet exists. In the past few years, a number of technical developments have taken place that might permit the establishment by the 1990s of an observational system approaching these requirements. We focus here on two major components of such a hypothetical system: ocean acoustic tomography, and satellite observations of sea surface topography and of wind stress. These, combined with other types of observations and with a sensibly designed modelling effort, might provide an ocean-observing system at not unreasonable cost. This would lead to significant progress in ocean physics and dynamics, and one could contemplate real-time forecasting for ship routing, military purposes, fisheries, weather, and climate.

1. Introduction

Looking back over the last 30 years at our evolving ability to observe the fluid ocean, one is impressed by the enormous progress made, but dismayed by the continuing mismatch between what is possible and what is necessary. In general terms, the history of oceanographic observation can be divided into two periods of differing emphases. The first period is conveniently, if imperfectly, dated from the H.M.S. *Challenger* expedition of 1872 (see Deacon (1971) for a historical account). This was the period of exploration by ships of the large-scale features of the ocean. It led to the hydrographic mapping of the temperature, salinity and density features associated with the dominant ocean currents. The primary instrument for this work was the ship itself. This form of observation is by no means obsolete: the equatorial undercurrents were not discovered (or rediscovered) until 1952, and some of the deep western boundary currents are being examined now for the first time (Warren 1981). Still one could fairly characterize this first period of oceanography as a 'century of undersampling'. Measurements from a moving vessel give neither a time series at a fixed coordinate nor a synoptic map, and some of the most important and energetic features of ocean dynamics (e.g. the mesoscale eddies) fell through the gaps of the traditional observational efforts.

The advent of modern pressure-vessel technology, electronics and computers have now made possible the acquisition of oceanographic *time series* on a sustained basis. (Some notable time series from ships had been collected by Pillsbury (1891) and Ekman (1953), but these were almost in the nature of *tours-de-force*.) By the early 1970s oceanographers were in a position to deploy arrays of instruments (both moored buoys and free-floating drifters) for the study of space and time scales over substantial regions. Baker (1981) has provided an interesting review of these developments. By the mid-1970s physical oceanographers had tended to shift away from large-scale survey

† On leave from Scripps Institution of Oceanography, La Jolla, California, U.S.A.
‡ On leave from Department of Earth and Planetary Sciences and Department of Meteorology and Physical Oceanography, Massachusetts Institute of Technology, Cambridge, Massachusetts, U.S.A.

oceanography toward exploiting these new capabilities. The resulting period can, with some oversimplification, be considered the era of regional dynamical oceanography, with emphasis on physical processes (internal waves, mixing processes and mesoscale variability) over substantial areas, but areas still much smaller than ocean basins.

The impact of this most recent period has been profound; we now appreciate that the ocean is a three-dimensional turbulent fluid with movement and variability on all space and time scales. One suspects, as with other turbulent fluids, that different components of the flow are strongly coupled. This coupling is not only between widely separated temporal and spatial scales, but also between remote geographic locations.

From the vantage point of the early 1980s, we can now appreciate the magnitude of the job facing oceanographers who wish to understand how the ocean 'works', and who might one day hope to forecast changes in ocean conditions. The ocean is a global fluid, not unlike the atmosphere, and one wishes to observe the global system on all important space and time scales.

The oceanographers' problem today is that there is only one instrument capable of covering the ocean globally: it is still the ship. The fundamental problem with ships (apart from their costs), is that they are intrinsically mismatched to observing a global, changing fluid. By the time one has covered even a tiny fraction of the ocean with all the ships available to oceanographers, the system has changed. Ships by their very nature time-alias the fluid.

We do have moored and freely drifting instruments capable of observing the short time scale variability of the ocean. For studying the large-scale movement of the sea, we believe that we must deploy instruments roughly every 50 km horizontally and 0.5 km vertically. Such deployments have in fact taken place in the regional experiments of the past decade. But the number required to cover a global ocean this way is prohibitive in both financial and human terms.

This is the puzzle facing oceanographers: how does one observe a global fluid on sufficiently fine space and time scales? We note that the analogous problem has been solved, at least partly, for the meteorologists because national governments have felt compelled to forecast the weather. The global observing systems available to meteorologists are mainly the sum of such national efforts and a by-product of them. National governments have never felt obliged to forecast conditions in the ocean; although one may argue that such an interest should be there, it will probably develop only after the virtues of such a capability have been demonstrated.

Oceanic observations lie primarily in the hands of small private or quasi-governmental institutions like Woods Hole Oceanographic Institution or the Institute of Oceanographic Sciences. Consider the corresponding situation in meteorology if the operators of the global network similarly consisted of a few professors. During the Easter vacation, after great fund-raising efforts, they would bring together their graduate students, a few balloons, radiosondes and barometers, and deploy them in a small array across the British Isles for a week or so. They would then pack up and analyse the data for a year before attempting to try again somewhere else. Occasionally, in a fit of great energy, some small group would drive across the European continent in a caravan of automobiles, stopping every few hundred kilometres to release a radiosonde and read a barometer.

The situation facing oceanographers is not so very different. Even if an international ocean observation network were established, we doubt that this could do the job if it were based on the proliferation of present systems.

PHILOSOPHICAL TRANSACTIONS OF THE ROYAL SOCIETY A MATHEMATICAL, PHYSICAL & ENGINEERING SCIENCES

2. Some recent developments

We shall describe two complementary observation systems that have been sufficiently developed that by the 1990s they, or something like them, could go a long way toward solving the global observation problem. We do not mean to imply that there are no other possibilities, nor that some as yet unforeseen technical development will not transform our existing capabilities (what oceanographer in 1940 would have predicted the transistor?), but only that we can see the outlines of a possible system that could solve many of our problems.

A condition underlying any ocean observing system is that the ocean is transparent to sound, but opaque to electromagnetic radiation. The first system, which we call ocean acoustic tomography, measures what happens *within* an ocean volume by transmitting sound *through* this volume along many different paths. It is analogous to the medical procedure called computed tomography (c.t.): sectional X-rays taken from many angles are processed by computer to yield a two-dimensional display of the interior structure. The second system, involving satellites, recognizes explicitly that only surface information is obtainable from electromagnetic space probes, but measures the appropriate quantities that allow sensible downward inferences. The two systems are complementary.

In order to focus this paper, we shall assess how these observational systems could be applied to just a few of the outstanding issues in large-scale oceanography. The list is not inclusive, merely illustrative. It is biased toward scientific climate-oriented problems.

3. Problems of gyre-scale oceanography

The past few years have seen a revived interest in the study of the ocean circulation and its fluctuations on the largest scales. We can trace this renewed interest to a number of disparate causes. First, a sense that the mesoscale variability (Mode Group 1978) which engaged so many oceanographers over the past decade is now somewhat understood. Second, the development of new analytical methods (beta spirals, inverse methods, and the like) for dealing with large-scale hydrography. Third, the existence of large-scale, eddy-resolving circulation models that are looking increasingly realistic. Fourth, the belief that ocean variability may play a decisive role in climate fluctuations, and the realization that our picture of the large-scale ocean circulation remains only qualitative, owing to a paucity of observations.

One would like to measure a number of important physical parameters on the gyre scale for long periods of time. We list some of the key parameters and the reason for their importance.

3.1. *Temperature*

The heat content of the ocean varies with position and time. Determining the seasonal cycle of heat storage is important for understanding the present-day circulation and its effects on climate. Interannual variability of heat storage, if it is significant, could result in an indicator of a changing climate. Similar trends in the average temperature of deep water would almost certainly be taken as an indicator of climatic change. The stability of the deep water to short-period fluctuations, as opposed to that of the shallow ocean and atmosphere, makes it a suitable place to look for early evidence of a general warming associated with the increase in atmospheric CO_2. The deep signal is small, but so is the background noise. From the work of Hansen *et al.* (1981) and Gornitz *et al.* (1982), one might infer that by now the warming of the oceans at 1 km depth amounts to a few millikelvins per year.

3.2. *Heat flux*

Meridional heat flux in the ocean and its variability may be crucial to an understanding of present-day climate and climatic changes. A determination of heat flux would offer an integral constraint on the rate of water mass formation and conversion as part of the global ocean circulation. Water mass formation rates and the implied mixing mechanisms are of importance both in understanding the general circulation, and in making forecasts – such as the uptake of CO_2 by the ocean, the response of the ocean to an atmospheric temperature rise, and the fate of radioactive wastes discharged into the ocean.

3.3. *Currents*

There is no need to belabour the importance of measuring the large-scale velocity field of the ocean. Any claim to understanding how the gyre-scale circulation works must contain a three-dimensional picture of the flow field and its relation to heat and salt fluxes.

3.4. *Vorticity*

The geostrophic velocity balance is indifferent to sources and sinks of energy and momentum. Only by examining the vorticity balance can one infer the input of momentum and energy into the ocean. We note that crucial concepts such as the Sverdrup vorticity balance (Stommel 1965) still remain highly problematical; they have never been tested by direct measurement.

Most of the vorticity changes on short time scales (a few months) may be caused by the advection of mesoscale eddies into and out of an observation area. There will be a tendency towards vorticity cancellation through the random summation of eddies with cyclonic and anticyclonic vorticity. On the longer time scales we may expect the Sverdrup (planetary) vorticity balance to dominate, and we can anticipate an annual cycle and possibly an interannual variability.

3.5. *Upwelling*

The gross pathways by which the cold water formed at high-latitude sinking regions manages to upwell into the interior thermocline of the ocean are known only sketchily from theory (e.g. the Stommel & Arons (1960) model), or from rather worrisomely oversimplified chemical-box models. Very little is known as to where and at what rate the cross-isopycnal (diapycnal) flows occur, and the extent to which such flows have annual and interannual variations.

4. Ocean acoustic tomography

Ocean acoustic tomography was proposed by Munk & Wunsch (1979), and was demonstrated in three dimensions at sea in 1981 (Ocean Tomography Group 1982). Perturbations in travel time of acoustic pulses can be interpreted in terms of perturbations in temperature, density and velocity. The geometry is displayed in figure 1. Each of S sources transmits to each of R receivers; for each of the $S \cdot R$ source–receiver pairs there are P distinct ray paths, some steep (and thus 'sampling' the ocean from top to bottom) and others flat (remaining near the sound axis at about 1 km). Application of inverse theory converts the data set consisting of travel times to a mapping of the intervening ocean volume. The information grows as $S \cdot R$, compared with $S + R$ for conventional moorings. The observations are inherently path integrals in which the small-scale fluctuations are suppressed. For further discussion we refer to Munk & Wunsch (1979, 1982*a*, *b*).

Spiesberger *et al.* (1980) demonstrated the resolution and stability of ray paths over a megametre

range (1 megametre (Mm) = 1000 km). The 1981 experiment was across a 300 km square, but included some remote receivers at megametre ranges.

At present, there are two types of tomography. The first relies upon measuring the travel time from source to receiver, and is a measure largely of temperature fluctuations in the ocean ('temperature tomography'). This was used in the 1981 demonstration. The second relies on the *difference* in the two-way travel times between co-located sources and receivers, and is a direct

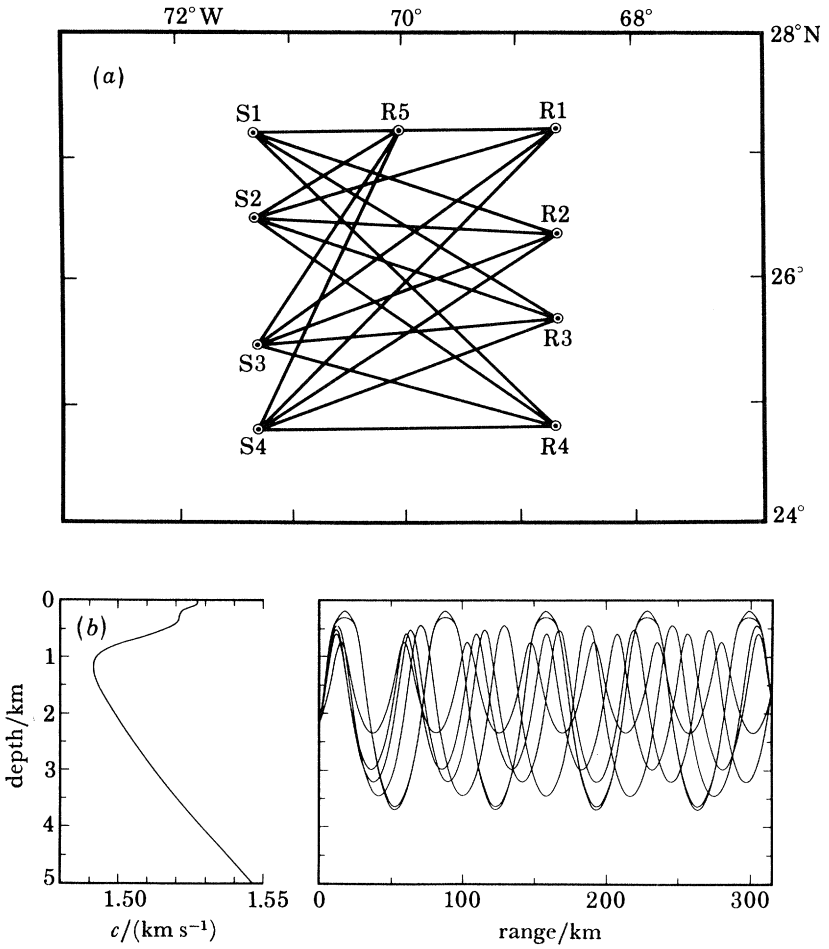

FIGURE 1. Geometry of the tomography demonstration experiment (Ocean Tomography Group 1982). There are 20 paths between four sources and five receivers (*a*) for each of these paths there are 5 to 10 ray multipaths depending on the local sound speed profile (illustrated in (*b*) for S1 to R3, upward launch angle only). Perturbation in travel time along the 100 or so paths *through* the ocean volume are used to infer sound speed (temperature) perturbation *within* the volume. This 'temperature tomography' can be extended to 'velocity tomography' by using the differences in travel times along oppositely directed transmissions between co-located sources and receivers.

measure of the velocity component lying in the vertical plane connecting the acoustic instruments. The only demonstration so far is the 25 km reciprocal experiment of Worcester (1977); a test at 300 km will occur in 1982 and a megametre reciprocal transmission is planned for 1984. We refer to this type as 'velocity tomography'. 'Tomography' encompasses both types. (In velocity tomography for N moorings with co-located sources and receivers there are $\frac{1}{2}N(N-1)$ reciprocal paths.)

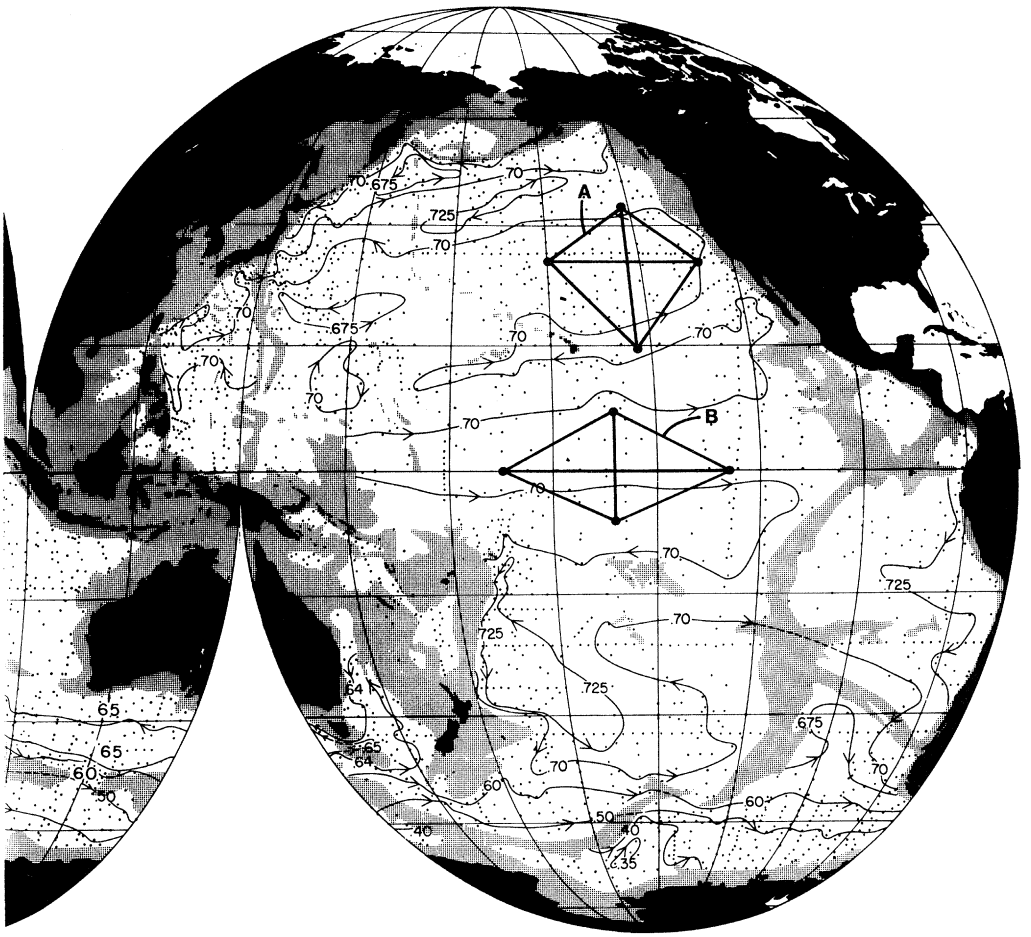

FIGURE 2. Possible subtropical (A) or equatorial (B) arrays in the eastern Pacific, on a 2500 km scale. Co-located sources and receivers permit temperature and velocity determination along six paths. Vorticity can be determined within each of the four sub-triangles, as well as within the entire diamond array. (Chart from Reid (1981).)

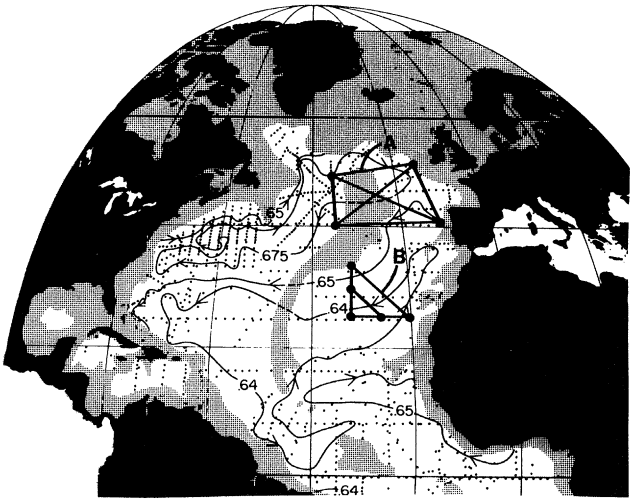

FIGURE 3. (A) Four-point subpolar array in the North Atlantic. (B) A mooring array in the eastern Atlantic basin for studying the vorticity balance (beta spiral).

For the 1981 experiment the travel times were used to map the variable field of sound speed (temperature) in the 300 km × 300 km × 5½ km ocean volume. In effect, the integrated measurements were differentiated to yield resolution at about a 50 km scale. A megametre array in the subtropical gye of the eastern Pacific is planned for 1984 to exploit the integrating properties of the measurements.

For observing the oceans in the 1990s, we focus on a 2500 km square array in the subtropical gyre of the eastern Pacific (figure 2). (Other possibilities include a tropical array and a sub-polar array (figure 3).) The 2500 km scale is an ambitious but rational extrapolation of developments so far (appendix A). Measurements given the mean properties along the four sides and the two interior diagonals.

The advantages or disadvantages of tomography as a tool for providing large-scale (and hence climatological) data can be summarized as follows.

Advantages

Large-scale spatial integration; information increases geometrically with the number of moorings; unattended recording over a year or more (⅓ year demonstrated so far); submerged instrumentation (of especial interest in regions of seasonal ice formation); remote sensing (of potential use in regions of strong currents); good vertical resolution.

Disadvantages

Sound speed is not a unique measure of temperature or density. However, in regions with stable temperature–salinity relations the separate temperature and salinity fields (and hence the density field) can be inferred to adequate precision (Cornuelle 1982). We shall assume that this can be done.

4.1. *Temperature*

An analysis of the errors in a temperature measurement is fairly straightforward and is given in appendix A. The conclusion is that changes by 10^{-3} K (1 mK) in the average along a 2500 km path could be detected. At 2500 km distances, we expect to be able to resolve a minimum of 15 ray paths, corresponding to a vertical resolution of 100 m at the base of the mixed layer (Munk & Wunsch 1982*a*) and 1000 m in the abyssal ocean.

Thus we can map the mean heat content in the box as a function of depth and time. Because of the large dimensions of the box, the 'noise' associated with mesoscale eddies is greatly subdued. Upper and lower bounds to the heat content can be computed with the extremal methods of inversion described by Wunsch & Minster (1982). These procedures provide a stable estimate of the bounds, given the vector of measurement error.

4.2. *Heat flux*

Velocity and temperature tomography give estimates of $\bar{u}$ and $\overline{T}$. One would like to infer the total heat flux $\overline{uT}$. With a sparse array like the one we are considering, there are three related approaches to this problem. The first involves the use of numerical models, e.g. the type described by Semtner & Mintz (1977) (figure 4). Such models contain a great deal of physics – including eddy fluxes – that cannot be dealt with analytically. One proceeds by requiring that the model be consistent with the integral properties (including $\bar{u}$ and $\overline{T}$), measured with the tomographic net. The model is then used to compute the eddy heat fluxes $\overline{uT}$. Like any other deductive calculation, the result is no better than the underlying model assumptions.

The second approach is more analytical. It is plausible that with known dynamics (like quasi-linear baroclinic Rossby wave dynamics), one can invert directly for $\overline{uT}$. We are optimistic about this approach because the thermal wind (explored in this context by Munk & Wunsch (1982*a*) is a relation between the velocity and temperature fields. As with any other inversion, the solution is non-unique, but techniques related to those described by Wunsch & Minster (1982) can provide useful bounds.

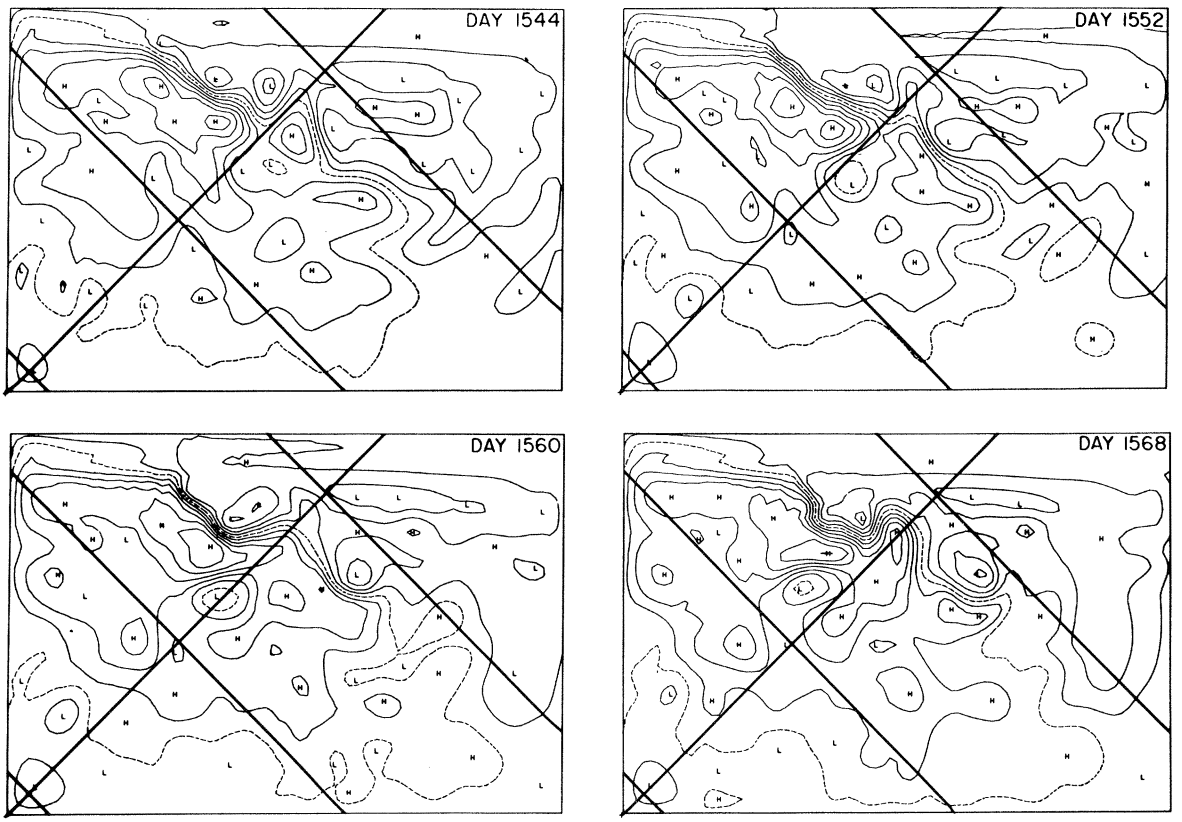

FIGURE 4. Four realizations of the 'eddy-resolving' circulation model of Semtner & Mintz (1977) at 8-day intervals. Contours of surface elevation (with 20 cm contour interval) are plotted. The intense snake-like flow is the model Gulf Stream. A strong time-dependent mesoscale eddy field is apparent. Such models are becoming more realistic and would be used in conjunction with the tomographic and satellite systems.

The third method relies on the non-reciprocity of two-way transmissions owing to currents. Perturbations in reciprocal travel times $\Delta_{\pm}(t)$ are proportional to $\delta C \mp u$; the difference in the variances, $\overline{\Delta_+^2} - \overline{\Delta_-^2}$, is proportional to $\overline{u\delta C}$, or nearly to the eddy heat flux $\overline{u\delta T}$. We can also obtain the total flux $\overline{uT}$. (See appendix B for the derivation.) The measurement is unorthodox in that it determines the heat flux *in* a plane, rather than the heat flux *across* a plane, and this raises problems with the interpretation of the mean component.

4.3. *Currents*

Our goal is to measure travel time to one part in 10^6, corresponding to measuring currents to 10^{-6} the speed of sound, or 1.5 mm s^{-1}. Standard current meters have precisions of 1 cm s^{-1}. However, the principal asset is not the precision but the large-scale spatial integration, and this leads us to the next topic.

4.4. *Vorticity*

Perhaps the most challenging application of the velocity measurement is to determine large-scale vorticity. This was suggested by Rossby (1975) but to our knowledge has never been done. By measuring the 'sing-around' travel times along the periphery of the proposed array, clockwise and anticlockwise, and forming the difference, one gets a direct measure of the total vorticity within the array. This can be done for each of the four interior triangles (three of which are independent) to obtain some information about vorticity gradients. One elegant feature is that the need for precise time-keeping is dispensed with in a sing-around geometry (appendix C).

Because tomography has the ability to resolve the ocean in the vertical, the vertical stucture of the mean vorticity can be combined with the vertical structure of the density field to yield potential vorticity as a function of depth. This type of information may provide very powerful constraints on analytical and numerical investigations of oceanic circulation. For reasons already stated in § 3.4, most modern theory is in terms of vorticity as the independent variable.

How accurately can we measure vorticity? Consider an $L \times L$ square. From Stokes theorem the circulation $4Lv$ equals $L^2\zeta$ where ζ is the mean vorticity in the square, and v is the mean velocity around the periphery. Thus $\zeta = 4v/L$. But $v/C = \frac{1}{2}\delta\Delta/\Delta$ where $\delta\Delta$ is now the difference in anti-clockwise minus clockwise sing-around time. We have given a somewhat optimistic argument that $\delta\Delta/\Delta$ can be measured to a precision of 10^{-6} independent of L (see appendix A). This corresponds to a vorticity

$$\zeta = (2C/L)\,(\delta\Delta/\Delta) = (1.2 \times 10^{-3})\,10^{-6} = 1 \times 10^{-9}\,\mathrm{s}^{-1} = 1 \times 10^{-5} f$$

for $L = 2500\,\mathrm{km}$ and $f = 2\Omega \sin(\text{latitude}) \approx 10^{-4}\,\mathrm{s}^{-1}$. The required mooring position-keeping is $10^{-6}L = 2.5\,\mathrm{m}$, and $\delta\Delta = 1.7\,\mathrm{ms}$.

What is the expected signal? In a Sverdrup balance

$$\rho\beta v h = \mathrm{curl}\,\tau,$$

where ρ is density, h is layer depth, $\beta = \mathrm{d}f/\mathrm{d}y$ (y is northward) and τ is the wind stress. Set $v = \partial_x\psi$, $\zeta = \nabla^2\psi$, $\beta = f/r_{\mathrm{Earth}}$. Let τ vary from $-\tau_0$ in the trades to $+\tau_0$ in the westerlies over a distance L. The resulting gyre vorticity is

$$\zeta_g = \nabla^2\psi = \psi_{yy} = 8xr_{\mathrm{Earth}}\tau_0/\rho L^3 h f = 10^{-8}\,\mathrm{s}^{-1} = 10^{-4} f$$

for $x = 3000\,\mathrm{km}$ designating the distance from the eastern boundary, $L = 2500\,\mathrm{km}$, $h = 1\,\mathrm{km}$, $r_{\mathrm{Earth}} = 6000\,\mathrm{km}$, $\tau_0 = 1\,\mathrm{dyn\,cm^{-2}}$ ($10^{-5}\,\mathrm{N\,cm^{-2}}$), and $f = 10^{-4}\,\mathrm{s}^{-1}$. This is ten times our precision estimate.

The mean vorticity in a mesoscale eddy might be $\zeta_e = 10^{-1} f$, and so be enormous compared with the gyre vorticity $10^{-4} f$. However, with $L_e = 100\,\mathrm{km}$ and $L_g = 2500\,\mathrm{km}$, the eddy integrated vorticity $L_e^2\zeta_e$ might be about the same as the gyre $L_g^2\zeta_g$, and we can expect a significant fluctuation in the measured circulation as mesoscale eddies enter and exit the array area.

For an array consisting of n peripheral transducers, Longuet-Higgins (1982) has shown that $n(n-1)/1 \times 2$ is the number of paths between instrument pairs, $n(n-1)\,(n-2)/1 \times 2 \times 3$ is the number of triangles, and $(n-1)\,(n-2)/1 \times 2$ is the number of independent triangles. For a square array (figure 2) there are six travel paths (and thus twelve independent reciprocal transmissions) and four triangles, but only three of the triangular sing-arounds are independent (since $\Delta_{1231} + \Delta_{1341} = \Delta_{12341} = \Delta_{4124} + \Delta_{4234}$). For a pentagonal array we get six independent measures of vorticity, enough to determine the coefficients in a power-series expansion (with subscripts designating differentiation)

$$\zeta = a + b\zeta_x + c\zeta_y + d\zeta_{xx} + e\zeta_{xy} + f\zeta_{yy},$$

so one might consider a vorticity balance

$$(\partial_t + v\cdot\nabla - A\nabla^2)\,\zeta = \operatorname{curl}\tau,$$

with the terms on the left-hand side acoustically measured, except for the diffusivity A.

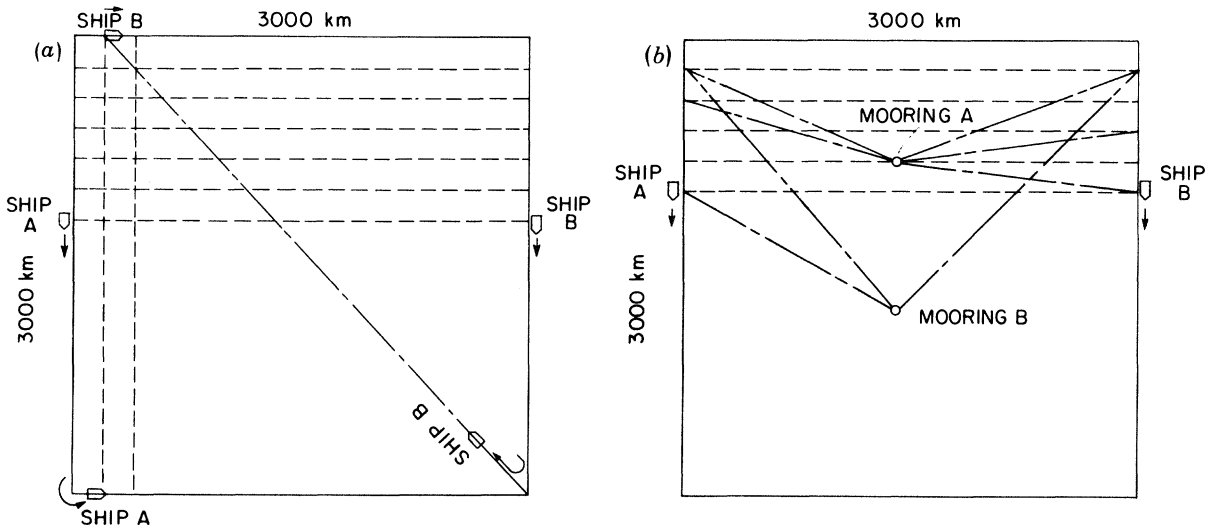

FIGURE 5. Ship-to-ship tomography over a large area. This requires very precise navigation, as may become available from the Global Positioning System in the mid-1980s. For two ships stopping every 50 km for 30 min (this may not be necessary), a tomographic coverage with 100 km resolution is completed in 13 days (*a*). The combined ship-mooring tomography (*b*) increases the number of transmission paths from one to six, and greatly reduces the coverage time.

4.5. *Upwelling*

The ability to measure velocities and densities over moderate-sized regions of the central ocean permits a connection to be made to ordinary vorticity dynamics and leads to an ability to infer vertical velocities. The condition of non-divergence states that

$$u_x + v_y + w_z = 0.$$

Conservation of density requires that

$$u\rho_x + v\rho_y + w\rho_z = 0.$$

Thus with an array like B of figure 3 we can estimate w or w_z. In practice one would solve for both w and w_z by inverting the two equations simultaneously. We estimate that w as small as $10^{-5}\,\mathrm{cm\,s^{-1}}$ (*ca.* $1\,\mathrm{m\,d^{-1}}$) would be measurable, a value representative of open sea upwelling.

The density conservation equation can be written

$$-w = u(\rho_x/\rho_z) + v(\rho_y/\rho_z) = -uh_x - vh_y,$$

where h_x and h_y are the slopes of isopycnal surfaces (in the notation of Stommel & Schott 1977). Combining this with the linear quasi-geostrophic momentum balance equations leads to the beta-spiral equation

$$uh_{xz} + v(h_y - \beta z/f)_z = 0.$$

All these terms can be measured, at least in principle, and so the beta spiral provides a set of consistency relations that are useful in the inversions.

4.6. *Further developments*

As the Global Positioning System (GPS) (see Klepczynski 1978) becomes operational, the possibility for doing acoustic tomography from ships is opened up. The GPS level of accuracy in

navigation (*ca.* 1 m horizontally) would remove the ship position error from the measurement, provided that towed sensors (perhaps arrays) can be navigated relative to the ship with high accuracy. One could envisage ship-to-ship tomography (figure 5*a*) or a mixed ship-to-mooring tomography (figure 5*b*), permitting rapid mapping of large ocean areas. This would eliminate clock and power problems, but with the present arrangement a high processing gain is achieved by many repetitions of the coded sequence in a single transmission; travel-time precision and path stability is attained by averaging many such transmissions. There is a question of how all this can be done in a moving geometry.

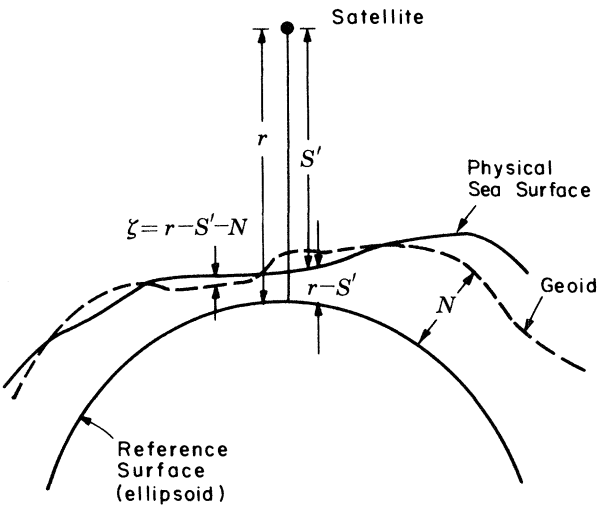

FIGURE 6. Altimeter determination of surface topography ζ and surface pressure $\rho g\zeta$ associated with ocean circulation. A satellite with a microwave altimeter is flown at an altitude of about 1000 km, and tracked with high accuracy. The difference between the tracking height r and the altimetric height S' gives the physical elevation of the sea surface. The appropriate equipotential surface (the geoid N) is then subtracted, leaving the elevation ζ associated with geostrophic surface currents.

Long-range tomography demands low-frequency broadband sources. A number of approaches to this problem are being taken. They range from state-switched sources to exponential or near-exponential horns. Any solution must be cheap, and easily handled at sea.

Large-scale tomographic systems require access to the data without the necessity of recovering the instruments (if only to monitor system performance). Military or weather-forecast applications, or both, require timely readouts. Two possibilities are being explored: (i) acoustic telemetering to shore stations (F. Birdsall, personal communication), and (ii) relay through the sea surface to satellites (J. Dahlen, personal communication).

5. SATELLITE ALTIMETRY AND SCATTEROMETRY

Various types of satellite measurements of the ocean have been available for nearly 20 years. Most of the measurements here consisted of infrared determinations of the sea-surface skin temperature. There is an important correction associated with atmospheric water vapour, but even if this correction can be made, the data are of only limited use to oceanographers. As a result of very complex air–sea transfer processes there is no simple connection between the infrared skin temperature and the temperature even 1 m below the surface. Consequently the infrared satellite

observations do not bear directly on the problem of gyre dynamics; but they do and will continue to give information on air–sea transfer processes, which play an important role in the thermodynamics of atmosphere and ocean, and in the salt dynamics of the ocean.

There are two recent developments in satellite technology that can be related more directly to the overall ocean dynamics. SEASAT (Born *et al.* 1979; Barrick & Swift 1980 and its immediate predecessor GEOS-3 (Douglas & Gaborski 1979) demonstrated the ability to measure from space the absolute shape of the sea surface, and the wind stress exerted by the atmosphere on the ocean (and vice versa).

5.1. *Altimetry*

The procedures for determining the absolute slope of the ocean surface, and its connection with the ocean circulation, have recently been described in some detail (TOPEX Science Working Group 1981; European Space Agency 1980; Wunsch & Gaposchkin 1980). We fly an altimetric satellite at about 1000 km above the Earth's surface (figure 6). Let S' be the distance from the satellite to the sea surface, r the distance of the satellite above a reference ellipsoid (as determined by a tracking system), and N the elevation of the geoid relative to the ellipsoid. (The geoid is that particular gravitational equipotential to which the sea surface would conform if the sea were brought to rest with no forces acting on it.) Then

$$S = r - S'$$

is the physical shape of the sea surface and

$$\zeta = S - N$$

is the shape of the sea surface relative to the geoid. The dynamic balance appropriate to large-scale quasi-geostrophic motion near the surface is between the horizontal gradient of $\rho g \zeta$ (g is the acceleration due to gravity) and the Coriolis force (Pedlosky 1979). The important consideration is the error budget in measuring ζ. Sources of error are as follows (TOPEX Science Working Group 1981).

(*a*) *Altimeter noise*. The accuracy of the altimeter flown on SEASAT approaches 5 cm, with a precision approaching 1 cm (Townsend 1980). (Altimeters with even better performance have been designed.) These instruments are a remarkable technical feat, and the 5 cm accuracy is the one most often mentioned in discussions of satellite altimetry. Unfortunately, it is not the limiting error.

(*b*) *Orbit radius* uncertainties arise from a variety of causes. If the spacecraft were globally tracked, the uncertainty in the oribit would be that of the tracking system. As it is, most spacecraft have been locally tracked by lasers, which provide only limited coverage owing to rather small numbers of stations, and the restriction to cloud-free periods. Orbit calculations are made by combining the sparse tracking data with the equations of orbit dynamics. The important errors are due to uncertainty in the Earth's gravitational field and unpredictable effects of atmospheric drag. Solar and Earth's albedo radiation pressures are not negligible. By careful study of the SEASAT tracking data, using the best available geoid, the random error is now estimated at less than 50 cm for each pass. In future missions this can be reduced to less than 10 cm by a combination of truly global, all-weather tracking from the Global Positioning System, through improvements in the knowledge of the Earth's gravity field both from existing data and from special-purpose gravity measuring satellite missions (TOPEX Precision Orbit Determination Group 1980; Jekeli & Rapp 1980), and through existing knowledge of the ocean circulation (Wunsch & Gaposchkin 1980) and its variability.

PHILOSOPHICAL TRANSACTIONS OF THE ROYAL SOCIETY A MATHEMATICAL, PHYSICAL & ENGINEERING SCIENCES

(*c*) *Tides*. Altimetric satellites can detect tides (Cartwright & Alcock 1981). Existing numerical tidal models (see, for example, Schwiderski 1980) have an accuracy approaching 10 cm in the well measured oceans. Improvements in the numerical models, long-duration altimeter missions, and a few well chosen tidal measurements *in situ* will probably remove the tides as a significant source of error (and will incidentally determine the global distribution of tides).

(*d*) *Wave bias*. The sea surface is a rough, moving, random field. Wave crests tend to be steeper than wave troughs; the altimeter pulse reflects more efficiently from the troughs, leading to a negative bias in surface elevation. This bias appears to be about 5 % of the r.m.s. wave height. The problem is solved by measuring the wave height with the altimeter itself (see Walsh *et al.* 1978), and making a bias correction (incidentally yielding global wave maps as a useful benefit (Chelton *et al.* 1981).

(*e*) *Atmospheric water vapour* affects the index of refraction of the atmosphere, delaying or advancing the time of arrival of the altimeter pulse. The problem is solved by measuring the water vapour directly from the spacecraft (Moran & Rosen 1980; Goldhirsh & Rowland 1980), thus reducing the error to a few centimetres.

(*f*) *Ionospheric electron content* in the ionosphere affects the effective index of refraction. The error is corrected both through models of the ionosphere electron content and by operating an altimeter at two frequencies (incidentally yielding ionospheric maps). The methods and errors are discussed by Davies *et al.* (1977) and Goldhirsh & Rowland (1980).

(*g*) *Atmospheric pressure loading*. The open sea is known to respond nearly isostatically to changes in atmospheric pressure ($-1\,\mathrm{cm\,mbar^{-1}}$ ($1\,\mathrm{mbar} = 10^2\,\mathrm{Pa}$); the inverted barometer effect). It appears that conventional surface meteorological analyses will be adequate to reduce this error to a few centimetres (there may be difficulties in intense storm systems).

(*h*) *The geoid* error enters the calculation of $\zeta = r - S' - N$ in two ways: as an error in the satellite orbit r (described in (*b*)) and as an error in the geoid N. Traditionally the geoid has been determined from surface gravity measurements on land and sea; in some regions (especially the western North Atlantic) the regional geoid is well determined from shipboard measurements through Stokes's theorem (Marsh & Chang 1978; Zlotnicki 1982). For low-order spherical harmonics the geoid is determined by tracking satellites in low orbits (King-Hele 1976; Lerch *et al.* 1979). Roemmich & Wunsch (1982) discuss how to use the geoid for determining the ocean circulation when only the large-scale features are known. Special satellite missions are now planned that will substantially improve the geoid.

There is some difficulty in disentangling the geoid perturbations from those associated with the steady ocean circulations (Wunsch & Gaposchkin 1980). But the situation is much improved for studies of the ocean *variability*, because the geoid is not time dependent (apart from tides). Accordingly, proposed altimetric missions put the satellite into orbits for which the ground track repeats itself with high accuracy (*ca.* 1 km) every 10 days or so (figure 7). There are trade-offs between polar coverage, rate of repetition of the ground track, and the distance between tracks. The discrete sampling in time and space leads inevitably to aliasing errors.†

Figure 8 is a sketch of the frequency–wavenumber content of the ocean circulation, and the

† The geoid is of great importance in studies of the solid Earth. With an error of order 1 m, the marine geoid can be deduced simply by ignoring the ocean circulation (and 1 m is much smaller than the errors in pre-altimeter marine geoids). This is the procedure adopted by Chapman & Talwani (1979) and others. In the future, the best geoids will be constructed by an optimum combination of satellite orbit perturbations, satellite altimetry and surface gravity (Zlotnicki *et al.* 1982), corrected for ocean circulation. The results should be accurate to a few centimetres.

PHILOSOPHICAL TRANSACTIONS OF THE ROYAL SOCIETY A MATHEMATICAL, PHYSICAL & ENGINEERING SCIENCES

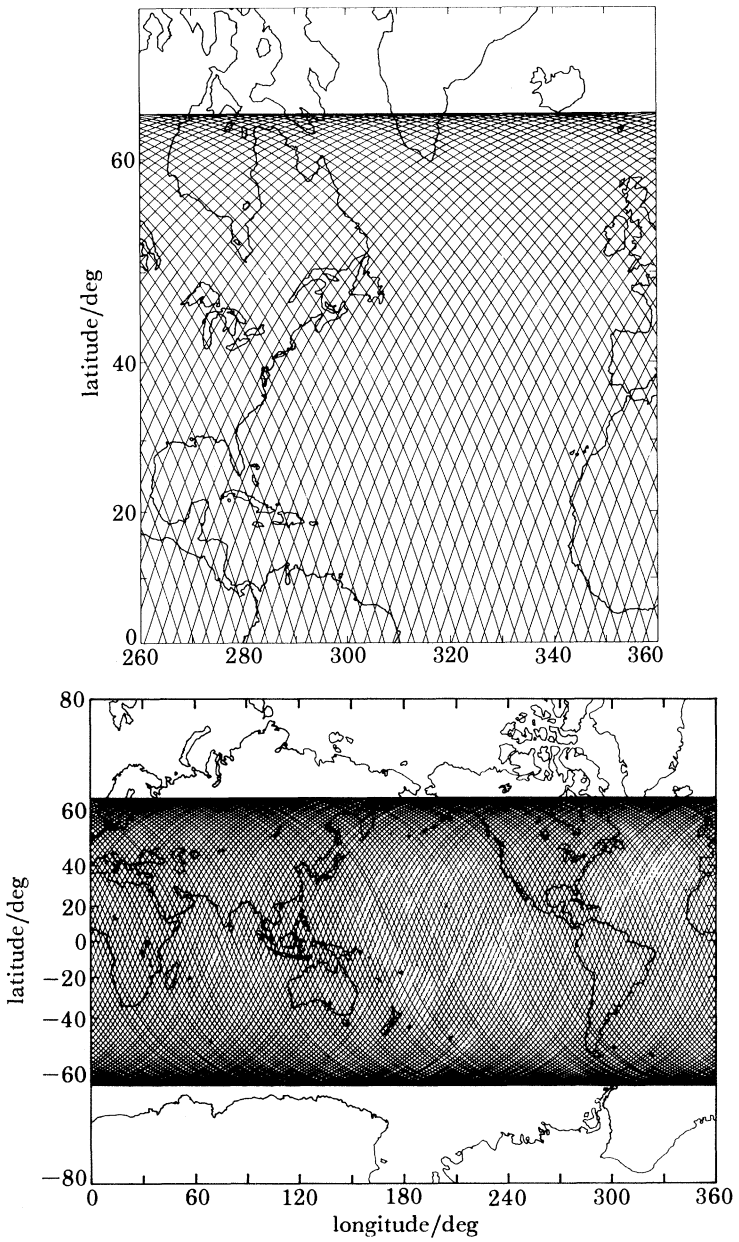

FIGURE 7. TOPEX ground-track coverage for each 10 day period for the North Atlantic and the world. Wind measurements would be obtained on similar space and time scales.

scales where various error sources are bothersome (although most are correctable). Orbit errors are important at large spatial scales, and geoid errors at large time scales. The error analysis indicates that for gyre scales (more than 1000 km, more than 1 month) one should be able to detect changes in sea surface elevation of a few centimetres or less.

5.2. *Scatterometry*

The determination of the vector wind stress, τ, acting on the ocean is one of the crucial problems facing oceanographers. Active microwave scatterometer systems have been demonstrated on

SEASAT as capable of useful accuracy and precision on a global basis (Jones *et al.* 1981). The scatter is from short capillary and gravity waves (Brown 1978; Barrick & Swift 1980; Johnson *et al.* 1980; Bracalente *et al.* 1980), and these are assumed to be in equilibrium with τ. The magnitude and propagation directions of these waves then lead to estimates of τ. The SEASAT instrument carried four dual-polarization antennas, each of which measured the radar backscatter coefficient in a different, downward looking, direction. This antenna geometry can lead to a fourfold ambiguity in wind direction. Work is now being directed at automatic algorithms for removing this ambiguity.

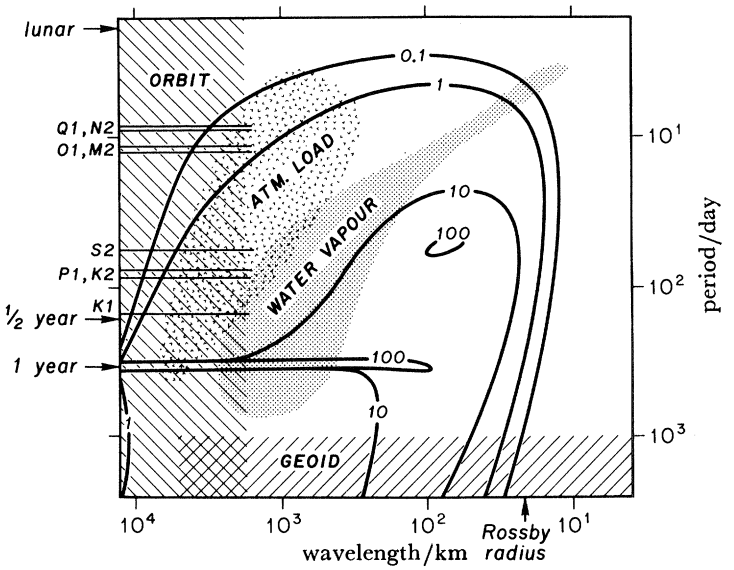

FIGURE 8. A schematic diagram of the frequency–wavenumber energy content of ocean circulation. Contours are proportional to energy density (in arbitrary units). Note the maximum at the one year period, and discrete spectral peaks (solid horizontal lines) at principal (aliased) tidal frequencies. There is a sharp decrease for scales smaller than the Rossby radius. The shaded areas give the (time and space) scales for which corrections for orbit and geoid errors; atmospheric water vapour content and atmospheric pressure loading are crucial. Almost all of these corrections can be applied, as described in the text.

The JASIN results (Chelton *et al.* 1981) provide the best available calibration of SEASAT scatterometry; for wind speed the accuracy was 1.6 m s^{-1}, and for wind direction 18° (aside from ambiguity), comparable with the best measurements *in situ*.

The important variable in large-scale circulation (vorticity) problems is not τ but curl τ, and this amplifies the high-wavenumber errors in τ. The same difficulty occurs with conventional wind measurements (Saunders 1976), and we do not yet know to what precision curl τ can be obtained from the scatterometry.

The coverage obtainable from scatterometry satellites is comparable with that for an altimetric satellite (figure 7). The European Space Agency (1980) report describes a specific proposal for wind measurements.

We can summarize the advantages and disadvantages of altimetry plus scatterometry, compared with conventional measurements *in situ*, as follows:

Advantages

Rapid global coverage; uniform global data sets; measurement of boundary conditions of dynamical equations (surface pressure gradient from altimetry, vorticity input from scatterometry).

Disadvantage

Measurement only at the upper boundary.

We now consider how the three-dimensional structure of the ocean can be inferred from measurements of pressure and wind stress at the upper boundary.

5.3. *Temperature in a linear, time-dependent ocean*

We already have a zero-order global picture of the temperature, salinity and thus density, structure of the mean ocean. Suppose that one can apply (at least locally) linear quasi-geostrophic dynamics (see, for example, Pedlosky 1979) to the time variability superimposed upon the zero-order climatology. Then, at least in principle, the measured surface pressure $\rho g\zeta(x, y, t)$ can be expanded in Rossby wave modes $p_r(x, y, 0, t)$ with modal frequencies and wavenumbers determined by the altimetric measurements. For each of these modes the interior pressure field $p_r(x, y, z, t)$ is then derived from Rossby wave dynamics, given only the zero-order buoyancy frequency $N(z)$ (see appendix D). The perturbation density field $\rho(x, y, z, t)$ is found from

$$-\rho g = \partial_z p = \partial_z \sum_r p_r$$

and is thus completely determined from the altimetry. In regions of stable temperature–salinity relations, the temperature can be inferred from the density field.

How well such a procedure might work in practice depends on the resolution and precision of the measurements and on the existing mode spectrum. In the western North Atlantic where the lowest baroclinic mode $r = 1$ contains about 90 % of the energy (McWilliams & Flierl 1976; Mode Group 1978), one obtains an adequate description by using $p = p_1$. The surface pressure field then is a direct mirror of the distortion of the main thermocline. Under these simplified circumstances the time-variable circulation (which is free of geoid error) on scales from 25 km to perhaps 3000 km has been determined from altimetry systems that have already been flown (see, for example, Gordon & Baker 1980; Cheney & Marsh 1981). There is evidence that the equatorial regions of the world ocean, and in particular the important El Niño region of the Pacific Ocean, can be described by this same type of physics, slightly modified for the equatorial waveguide (Leetmaa *et al.* 1981; O'Brien *et al.* 1980).

5.4. *Temperature in a time-averaged ocean*

There are several approaches here. The first is purely empirical: strong currents like the Gulf Stream have a strong baroclinic structure. Fuglister & Voorhis (1965) noted that the axis of the Gulf Stream can be well defined by the 15° C isotherm at 200 m depth. Given a measure of the surface elevation across the Gulf Stream, any experienced oceanographer could draw a rough picture of the corresponding isopycnal displacements. Empirical regression schemes could quantify the process and its errors.

A more interesting possibility is to use analytical solutions for the thermohaline circulation of the ocean (Welander 1971; Needler 1971). The problem is necessarily nonlinear, and involves an undetermined arbitrary function of the density field (appendix D). Under some circumstances, the satellite measurement of surface pressure and stress (and hence Ekman suction) could determine the arbitrary function. There is a fundamental question whether such thermocline models work. The existence of the mesoscale and of other oceanic variability implies that the mean ocean circulation is obtainable only as an average over many realizations. That average will introduce

PHILOSOPHICAL TRANSACTIONS OF THE ROYAL SOCIETY A MATHEMATICAL, PHYSICAL & ENGINEERING SCIENCES

eddy correlation (Reynolds stress) terms that do not appear in the existing thermocline theories.

The third, and most likely, procedure is to use the measured surface pressure and wind stress as boundary conditions in numerical models.

5.5. *Currents*

The surface geostrophic velocity $\boldsymbol{v}_s$ is related to the slope of the sea surface according to

$$-\hat{k}\times\boldsymbol{v}_s = gf^{-1}\nabla\zeta,$$

where ζ is the sea surface elevation relative to the geoid, as measured by satellite altimetry. Wunsch & Gaposchkin (1980) have shown that this is a practical method for measuring *absolute* geostrophic velocity, the variable component is easier to measure because it is free of geoid error (see, for example, Cheney & Marsh 1981).

The winds generate an Ekman flow $\boldsymbol{v}_E$ in the upper 100 m with a net transport τ/f to the right of the wind (in the Northern Hemisphere). This non-geostrophic component is invisible to the altimeter. The total flow $\boldsymbol{v}_s+\boldsymbol{v}_E$ can be obtained from a combined use of altimetry and scatterometry.

The *variable* velocity at depth can be inferred from a mode summation as with density, and subject to the same considerations. The *steady* flow at depth could be derived from the non-linear thermocline equations (see appendix D).

5.6. *Vorticity*

Here again linear dynamics (as in the normal mode summation) and nonlinear dynamics (thermocline theory) permit inferences of the time-dependent and time-independent vorticity at depth, given the vorticity input curl τ at the surface boundary.

5.7. *Upwelling*

The vertical velocity at the base of the Ekman layer is $\hat{k}\cdot\nabla\times\tau/f$. The vertical velocity at depth can be inferred from linear and nonlinear dynamics, as above, or from assimilation into numerical models.

6. Discussion

The superficial impression might be gained that the satellite and tomographic techniques provide separate, and even competitive, systems for observing the ocean structure. The point to be made here is that the systems are complementary, and that they can be used to mutual advantage. But no matter what the final system of data acquisition might look like, we can expect it to be assimilated into numerical modelling of the ocean circulation.

6.1. *A combined system*

Tomography can provide measurements of heat content, heat flux, velocity and vorticity. Altimetry and scatterometry provide surface boundary conditions. Consider first tomography used in the mapping mode, as in the 1981 demonstration experiment. Then because of the strong surface signature of mesoscale flow fields, satellite altimetry imposes severe constraints upon the acoustic inversion. Conversely, tomography provides the information for mapping of the altimeter and scatterometry data into a three-dimensional flow field.

We envisage that tomography in the 1990s is more likely to be used in the integrating mode rather than in the mapping mode. The horizontal resolution depends on the array dimension and

PHILOSOPHICAL TRANSACTIONS OF THE ROYAL SOCIETY A MATHEMATICAL, PHYSICAL & ENGINEERING SCIENCES

is likely to be poor, even though the number of paths grows geometrically with the number of moorings. But the vertical tomographic resolution of large-scale features is quite good, providing a dozen pieces of information on vertical structure at 2500 km ranges. For the satellite system, on the other hand, the vertical resolution is poor but the horizontal resolution is excellent. Time resolution is good in both systems, and there are some interesting trade-offs between space and time resolution of various satellite orbits. The complementary nature of the resolving powers of tomography and of the satellite measurements implies that a combination of these two disparate systems would be extremely powerful.

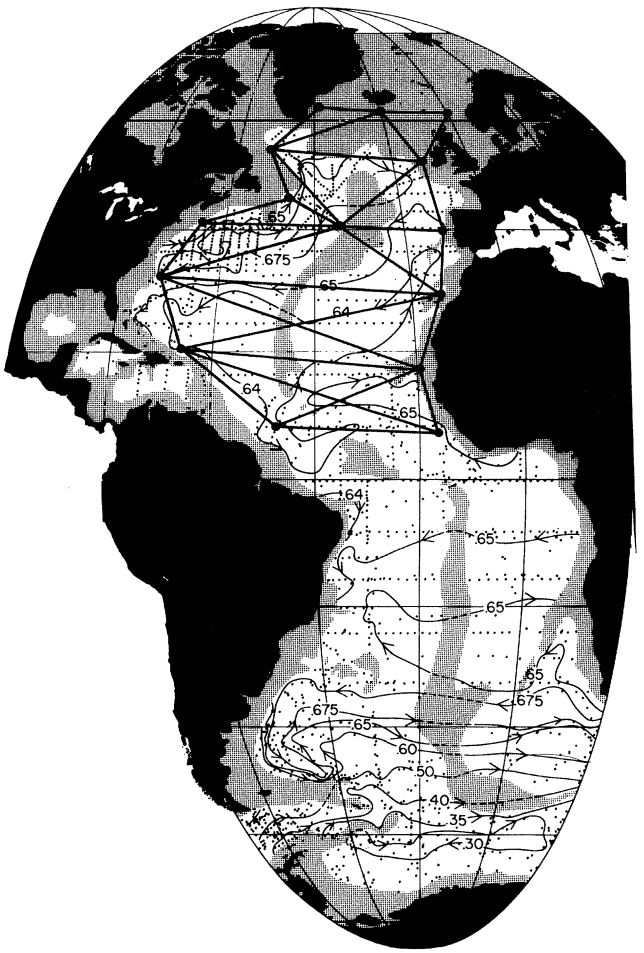

FIGURE 9. A 15 mooring tomographic array in the North Atlantic. Only the nearest-neighbour paths have been drawn. There are a total of 105 paths, and for each of these there are about 10 rays in the vertical plane. Tomography over such large distances requires further engineering developments. Data from this array and from satellite altimetry and scatterometry would be assimilated into a numerical model.

6.2. *Assimilation*

Figure 4 (from Semtner & Mintz (1977)) shows a modern eddy-resolving model of the ocean. Progress on these models is now very rapid. By the 1990s we expect to have realistic models for the major ocean basins.

Meteorologists are familiar with the process of assimilating into the forecast models observations every 12 h from the global meteorological network. (There are some pitfalls: see Ghil (1980).)

PHILOSOPHICAL TRANSACTIONS OF THE ROYAL SOCIETY A MATHEMATICAL, PHYSICAL & ENGINEERING SCIENCES

We envisage a similar process for the ocean models. Because of the longer time scales with the ocean we might get away with updates every one or two weeks. The observations to be assimilated into the models consist of wind stress and surface pressure derived from the satellite, of heat content, velocity and vorticity derived from tomography.

Figure 9 shows a possible tomographic array for the North Atlantic, to supplement the satellite surface coverage. Initially the model will serve to constrain and fill in the description of the variable ocean climate derived largely from the observational network. Later, the assimilated observations will serve to constrain the model description, and ultimately the model prediction. In this evolution from a data-intensive to a model-intensive mode, the key problem to be studied is the trade-off between model competence and observational hardware.

We are grateful to R. Revelle and P. Worcester for constructive criticism. The paper is an extrapolation of experience gained in a series of experiments and studies supported by the U.S. Office of Naval Research, the National Science Foundation and the National Aeronautics and Space Administration. Both of us acknowledge the support of Fulbright Awards, and one of us (C. W.) of a Guggenheim Foundation Grant during our stay at the University of Cambridge.

Appendix A. Precision and resolution at megametre acoustic ranges

The measurement error of arrival time for a resolved ray path is $(S/N)^{-\frac{1}{2}}\Delta$, where S and N denote signal and noise power, and Δ is essentially the reciprocal of the radiated bandwidth. Write $\Delta = Qf^{-1}$, where Q is the conventional 'Q' for a resonant source, and f is the centre frequency. For a 300 km transmission experiment in the fall of 1982 we have $Q = 4, f = 400$ Hz, hence $\Delta = 0.01$ s, and $S/N = 20$ dB, thus giving a measurement error of 1 ms, and a fractional error of 6×10^{-6}. Can this precision be retained at megametre ranges?

We wish to minimize $(S/N)^{-\frac{1}{2}}\Delta$. The signal intensity S is attenuated by α dB/km, with $\alpha \approx 10^{-7}(f/\mathrm{Hz})^2 \equiv \alpha_0 f^2$ below a few hundred hertz. This can be written $S/S_0 = \mathrm{e}^{-\beta R}$, with $\beta = \frac{1}{10}\alpha(\ln 10)$. At high frequency $S^{-\frac{1}{2}}$ is larger, and at low frequency Δ is larger (assuming constant Q). A minimum in $S^{-\frac{1}{2}}\Delta$ corresponds to a maximum in

$$S\Delta^{-2} \approx f^2 \exp\{-\tfrac{1}{10}(\alpha_0 R \ln 10) f^2\},$$

which yields an optimum frequency $f_{\mathrm{opt}} = (10/\alpha_0 R \ln 10)^{\frac{1}{2}} = 208$ Hz at $R = 1000$ km. Note that

Table A1. Acoustic transmission at 224 Hz over 1 Mm

(1) source level	189 dB/μPa	an array of sources at the same total level would yield a directivity gain of 3–5 dB
(2) spherical spreading	−120 dB	cylindrical spreading beyond 10 km gives −100 dB; our experience indicates that spherical spreading is more nearly correct.
(3) attenuation	−6 dB	
(4) receiver directivity	+4 dB	present configurations of four receivers
(5) coherent averaging	+16 dB	mean of 38 sequences
(6) pulse compression	+24 dB	for 225 digits per 8 s sequence, for a 32 Hz bandwidth†
	+107 dB	
(7) noise per hertz	−68 dB	medium shipping density at sea state 3
(8) bandwidth	−15 dB	for 32 Hz bandwidth†
(9) signal:noise	24 dB	
digit length	32 ms	for 32 Hz bandwidth
precision	1 ms	

† Bandwidth cancels between lines (6) and (8).

$\beta R = 1$ for $f = f_{\rm opt}$, so that the absorption is always by e^{-1} at the optimum frequency. Cylindrical spreading would reduce the intensity according to $S \approx R^{-1}$, and so the dependence of $S^{-\frac{1}{2}}\Delta$ on range (but always at optimum frequency) is

$$S^{-\frac{1}{2}}\Delta \approx R^{\frac{1}{2}} f_{\rm opt}^{-1} \approx R^{\frac{1}{2}} R^{\frac{1}{2}}.$$

The *fractional* error in travel time is independent of range. (All this is specific to a chemical absorption $\alpha \approx f^2$.) We have ignored the frequency dependence of the noise $N(f)$; at a few hundred hertz this is dominated by ship noise.

The conclusion is that the fractional travel time error (which is insensitive to range) is roughly 6×10^{-6}. Table A1 summarizes the expected performance. The table is based on conservative estimates. The precision can be further improved by using sources of greater power and shorter digit length, and the range extended from 1 to 3 Mm. For comparison, the fractional change in soundspeed is 3×10^{-6}/mK (for temperature tomography), and $7 \times 10^{-6}/(\mathrm{cm\ s^{-1}})$ (for velocity tomography).

Additional errors are introduced by timekeeping and mooring position keeping. Referring now to the experimental setup described by the Ocean Tomography Group (1982), clock error can be kept to 1 ms by use of a rubidium oscillator, and mooring motion can be monitored to 1 metre (corresponding again to 1 ms) by interrogating bottom transponders. These are acceptable errors.

Appendix B. Total heat flux from velocity tomography

Consider reciprocal transmissions along a ray path in the $\pm$ direction. Let

$$C(x,t) = C_0 + \delta C(x,t); \quad u = u_0 + \delta u(x,t) \tag{B 1}$$

designate sound speed and current component along the ray path. (Ray inclinations are small, and so u is essentially the x-component of horizontal current.) The fluctuating components are taken to have zero time average:

$$\overline{\delta C} = 0, \quad \overline{\delta u} = 0. \tag{B 2}$$

We further make a great simplification by assuming a homogeneous field of sound speed and currents, so that the mean values C_0 and u_0 are *not* functions of x.

Consider now the time-averaged C-flux

$$F \equiv \overline{uC} = u_0 C_0 + \overline{\delta u \delta C}. \tag{B 3}$$

For any given depth, C is nearly a linear function of temperature and depends only weakly on salinity, so that F is a measure of heat flux $\overline{uT}$. The two terms on the right-hand side give the contributions from the mean circulation and from the eddies, respectively. The eddy flux is a function of x, and we shall evaluate it as a ray average between sources and receiver. F is depth weighted in accordance with the fractional time spent by the ray at any given depth. By combining the results from many resolved rays, we can sort out the depth dependence and consider one depth layer at a time (Munk & Wunsch 1979, 1982*a*).

The travel time in the $\pm$ x-direction is given by

$$\Delta_{\pm}(t) = \int \frac{\mathrm{d}x}{C \pm u} \approx -\frac{1}{C_0^2} \int \mathrm{d}x(-C_0 + \delta C \pm u), \tag{B 4}$$

making use of $\delta C \ll C_0$ and $u \ll C_0$. We form the sum and difference of oppositely directed travel times:

$$\left.\begin{aligned} S = \tfrac{1}{2}(\Delta_+ + \Delta_-) &= -(1/C_0^2)\int \mathrm{d}x(-C_0+\delta C);\\ D = \tfrac{1}{2}(\Delta_+ - \Delta_-) &= -(1/C_0^2)\int \mathrm{d}x(u_0+\delta u). \end{aligned}\right\} \tag{B 5}$$

The time averages over a range R are

$$\bar{S} = R/C_0, \quad \bar{D} = -Ru_0/C_0^2, \tag{B 6}$$

so that the flux from the mean circulation is given by

$$C_0 u_0 = -R^2 \bar{D}/\bar{S}^3. \tag{B 7}$$

In the perturbation expansion (B 1), C_0 is operationally determined by $C_0 = R/\bar{S}$. There is an uncertainty in the location of moorings to ± 1 km, leading to an uncertainty in C_0 by one part in 3000, or ± 0.1 K in the absolute temperature, and a corresponding error in $\overline{uC_0}$ or $\overline{uT}$. As with any 'open' system, such a measurement of the mean flux is not readily interpretable. One must consider the observations in geometries in which total mass is conserved. This problem does not arise in the contribution from eddy fluxes $\overline{\delta u\,\delta C}$, which we consider next.

The 'propagation velocity' is

$$C_0 + v_\pm, \quad v_\pm = \delta C \pm u. \tag{B 8}$$

Travel time can be written

$$\Delta_\pm(t) = \int \frac{\mathrm{d}x}{C_0 + v_\pm} \approx \bar{S} - \frac{1}{C_0^2}\int \mathrm{d}x\, v_\pm(x). \tag{B 9}$$

We measure the time by which the arrival is *early*,

$$\delta\Delta_\pm(t) = \bar{S} - \Delta_\pm(t) = (1/C_0^2)\int \mathrm{d}x\, v_\pm(x),$$

with a mean-square value

$$\overline{(\delta\Delta_\pm)^2} = (1/C_0^4)\int \mathrm{d}x_1 \int \mathrm{d}x_2\, \overline{v_\pm(x_1)\, v_\pm(x_2)}. \tag{B 10}$$

Conditions have been assumed to be homogeneous, so that $\overline{v(x_1)\, v(x_2)}$ can be a function only of the separation $x' = x_1 - x_2$:

$$\overline{v(x_1)\, v(x_2)} = \overline{v^2}\rho(x'),$$

where $\rho(x')$ is the correlation, and $\rho(0) = 1$. Define an integral correlation scale

$$r = \int_{-\infty}^{\infty} \mathrm{d}x'\, \rho(x').$$

For mesoscale eddies $r = O$ (100 km). Under the condition that $r \ll R$, the x_1, x_2 coordinates can be replaced by x, x' coordinates, and the x' integration carried from $-\infty$ to ∞:

$$\overline{(\delta\Delta_\pm)^2} = \frac{\overline{v_\pm^2}}{C_0^4}\int_0^R \mathrm{d}x \int_{-\infty}^{\infty} \mathrm{d}x'\, \rho(x') = K\overline{v_\pm^2}, \quad K = \frac{Rr}{C_0^4}. \tag{B 11}$$

From the definition (B 8) of $v_\pm$,

$$\overline{(\delta\Delta_\pm)^2} = K\{\overline{(\delta C)^2} + \overline{u^2} \pm 2\overline{u\,\delta C}\}, \tag{B 12}$$

and so

$$\overline{u\,\delta C} = (1/4K)\,\{\overline{(\delta\Delta_+)^2} - \overline{(\delta\Delta_-)^2}\}. \tag{B 13}$$

PHILOSOPHICAL TRANSACTIONS OF THE ROYAL SOCIETY A MATHEMATICAL, PHYSICAL & ENGINEERING SCIENCES

The total flux (B 3) can now be written in the form

$$F = -\frac{R^2\bar{D}}{\bar{S}^3} + \frac{R^3}{r\bar{S}^4}(\bar{S}\bar{D} - \bar{S}\bar{D}).$$

The key result is that the mean of the product uC (and not just the product of the means) can be evaluated by using non-reciprocity as a novel geophysical tool. The mesoscale contribution to heat flux can then be determined in a long-range transmission, even though the mesoscale is not resolved.

One may prefer to express the results in terms of the spectrum

$$P_{\pm}(k) = \int_{-\infty}^{\infty} \mathrm{d}x' \, \mathrm{e}^{\mathrm{i}kx'} \overline{v_{\pm}(0)\, v_{\pm}(x')}$$

so that

$$P_{\pm}(0) = r\overline{v_{\pm}^2}. \tag{B 14}$$

The results are readily generalized to yield the spectrum of the eddy fluxes. We interpret equation (B 12) to apply to measurements of $\delta\Delta_{\pm}(t)$ through a narrow filter centred on frequency ω, and then repeat the analysis for many values of ω. (Alternatively one forms the cosine transforms of the lagged covariances; see Munk *et al.* (1981).) The relations (B 12) in spectral form now become

$$P(\delta\Delta_+\delta\Delta_+) = K[P(\delta C\delta C) + p(uu) + 2P(u\delta C)], \tag{B 15a}$$

$$P(\delta\Delta_-\delta\Delta_-) = K[P(\delta C\delta C) + p(uu) - 2P(u\delta C)], \tag{B 15b}$$

where the left-hand sides are the power spectra (or co-spectra) $P(\omega)$ of the measured time series $\delta\Delta_+(t)$ and $\delta\Delta_-(t)$, and the right-hand sides contain the field power spectra of $\delta C(t)$ and $u(t)$, and the co-spectrum of u and δC.

We can also form the co-spectra and quadrature spectra of the measured time series, and these are related to the field spectra as follows:

$$P(\delta\Delta_+\delta\Delta_-) = K[P(\delta C\delta C) - P(uu)], \tag{B 15c}$$

$$Q(\delta\Delta_+\delta\Delta_-) = KQ(u\delta C). \tag{B 15d}$$

The four equations (B 15) permit one to solve for the field spectra $P(\delta C\delta C)$, $P(uu)$, $P(u\delta C)$ and $Q(u\delta C)$. All spectra are of course functions of frequency.

We have here discussed the co-spectrum $P(u\delta C)$ as being related to the spectrum of eddy heat flux $P(u\delta T)$. Munk *et al.* (1981) were concerned with measuring ρuw, the vertical flux of horizontal momentum. But this is nearly $u\delta C$, since $\delta C = \mathrm{d}(\delta C)/\mathrm{d}t = w\,\mathrm{d}(\delta C)/\mathrm{d}z$. For a stationary process $P(m\dot{n}) = \omega Q(mn)$, and so

$$P(u\delta C) = (\omega C_0^2/rR)\, Q(\delta\Delta_+\delta\Delta_-). \tag{B 16}$$

Thus the quadrature spectrum of reciprocal travel times provides a measure of vertical momentum flux.

In the presence of shear, the reciprocal ray paths do not coincide. Roughly speaking, non-reciprocity can be ascribed to (i) the non-reciprocity of paths, and in particular to the difference in δC (which dominates u) along the two paths, and (ii) to travelling with and against the current u along the (undisturbed) path. We have ignored the former term as being of second order in most circumstances (but accountable with iterative techniques); the latter term is our signal.

Appendix C. Tomographic measurements of vorticity

The travel time from mooring i to mooring j is written

$$\Delta_{ij} = t_j - t_i + (\tau_j - \tau_i),$$

where t_i is clock time and τ_i is clock error for a transmitter at mooring i, and t_j, τ_j refer to a receiver at j. (True time is $t+\tau$.) Similarly for a transmitter at j and a receiver at i

$$\Delta_{ji} = t'_i - t'_j + (\tau_i - \tau_j).$$

The clock error drops out from the *sum* travel time (proportional to sound speed perturbation):

$$\Delta_{ij} + \Delta_{ji} = (t'_i - t_i) - (t'_j - t_j).$$

One can think of j as a transponder with a known delay $t'_j - t_j$, which has to be subtracted from the measured interval at mooring i between transmission time t_i and response time t'_i.

Clearly the clock error does not drop out from the difference $\Delta_{ij} - \Delta_{ji}$ (proportional to velocity).

But clock error does again drop out in a 'sing-around'. For n moorings around the periphery of an area, one has (setting the transpond delays to zero)

$$\Delta_{ij\ldots ni} = \Delta_{ij} + \Delta_{jk} + \ldots + \Delta_{ni} = t'_i - t_i.$$

$\Delta_{in\ldots ji}$ denotes sing-around in the opposite (negative) sense. This has two important connotations:

(a) $\Delta_{ij\ldots ni} - \Delta_{in\ldots ji}$ has no clock error;

(b) $\Delta_{ij\ldots ni} + \Delta_{in\ldots ji}$ has no clock error.

Condition (a) is of interest in connection with vorticity measurements; (b) is less familiar, but might also be useful as a measure of mean boundary temperature.

But *mooring motion* does not drop out for sing-arounds. Let $u_{i,\,ij}$ designate the drift velocity of instrument i in the direction ij, and U_{ij} the mean current (along the ray) from i to j. Then the range from transmitter i to receiver j is given by

$$R_{ij} = R_0 + u_{j,\,ij}\Delta = (C + u_{j,\,ij})\,\Delta,$$

and similarly

$$R_{ji} = R_0 - u_{i,\,ij}\Delta = (C - u_{i,\,ij})\,\Delta,$$

where $\Delta = R_0/C$ is the travel time uncorrected for drifts and currents. The precise reciprocal travel times (now neglecting clock errors) are

$$\Delta_{ij} = R_{ij}/(C + U_{ij}) \approx (C + u_{j,\,ij} - U_{ij})\,\Delta/C,$$
$$\Delta_{ji} = R_{ji}/(C - U_{ij}) \approx (C - u_{i,\,ij} + U_{ij})\,\Delta/C.$$

Hence

$$\Delta_{ij} + \Delta_{ji} = (2C + u_{j,\,ij} - u_{i,\,ij})\,\Delta/C$$

is independent of mooring corrections only if the two moorings swing together, $u_{i,\,ij} = u_{j,\,ij}$, whereas

$$\Delta_{ij} - \Delta_{ji} = (-2U_{ij} + u_{j,\,ij} + u_{i,\,ij})\,\Delta/C$$

measures the velocity U_{ij} relative to the mean motion of the moorings.

The only way out is to use very stiff moorings, or if necessary to measure the mooring motions (Ocean Tomography Group 1982). The mooring motion does of course drop out from averages over very many independent samples.

Appendix D. Inferences about the interior ocean from surface measurements by satellite

Consider a region of the ocean where linearized theory applies well to the time-dependent motions. Then over a flat sea floor the pressure field describing the three-dimensional fluid motion may be written (using F' for $\mathrm{d}F/\mathrm{d}z$)

$$p_r(x, y, z, t) = \lambda_r F_r'(z)\, P_r(x, y)\, \mathrm{e}^{-\mathrm{i}\omega_r t}. \tag{D 1}$$

The vertical wave functions $F_r(z)$ can be obtained from

$$F_r'' + (N(z)/\lambda_r)^2 F_r = 0 \tag{D 2}$$

subject to the boundary conditions

$$F = 0 \quad \text{on} \quad z = -D, \quad F' - g\lambda_r^{-2} F = 0 \quad \text{on} \quad z = 0, \tag{D 3}$$

where $N(z)$ is the buoyancy frequency, thus resulting in a Sturm–Liouville problem for linear Rossby waves. P satisfies a horizontal equation

$$L(P_r(x, y), \lambda_r) = 0, \quad P_r(x, y) = Y_r(y)\, \mathrm{e}^{\mathrm{i}k_r x}. \tag{D 4}$$

Note that each mode has its own characteristic wavenumber and frequency. If we can deduce ω_r, k_r from an altimetric measurement, we can determine $P_r(x, y)$ from the differential equation (D 4), and similarly F_r from (D 2) and (D 3). The pressure field is given by the mode summation

$$p = \sum_r p_r = \sum_r d_r F_r(z)\, Y_r(y)\, \mathrm{e}^{\mathrm{i}(k_r x - \omega_r t)} \tag{D 5}$$

and the perturbation density field ρ is found from

$$-\rho g = \partial_z p$$

and is thus completely determined from the altimetry. More complex but similar models can be used in regions of strong mean shear or bottom topography.

The *variable* velocity at depth can be inferred from a mode summation

$$\begin{Bmatrix} u_r \\ v_r \end{Bmatrix} = F_r'(z)\, \mathrm{e}^{\mathrm{i}(k_r x - \omega_r t)} \begin{Bmatrix} U(y) \\ \mathrm{i}V(y) \end{Bmatrix}$$

which is analogous to (D 1) for pressure (density), and subject to the same considerations.

In determining the time average density and velocity field, the practical approach is probably to use a numerical model and assimilation techniques. But an interesting analytical possibility is to relate the measurements to the thermohaline circulation models of the ocean (Welander 1971). According to Welander, there is an integral of the quasi-geostrophic equations of motion in the form

$$\sin(\text{latitude})\, \mathrm{d}\rho/\mathrm{d}z = G(\rho, p + \rho g z),$$

where G is an arbitrary function. Under some circumstances the satellite determination of surface pressure and stress (and hence Ekman suction) could provide information on the three-dimensional behaviour of G and hence of ρ, and the three components of velocity.

Although this is an interesting possibility to be explored, the existence of the mesoscale and other ocean variability raises fundamental questions. The variability induces eddy correlations

not appearing in the models. Measurements described in this paper could finally answer the question of whether the resulting eddy fluxes are important to the time-average flows. There is probably no substitute for good eddy-resolving general circulation models until the eddy processes are better understood.

References

Baker, D. J., Jr 1981 In *Evolution of physical oceanography, scientific surveys in honor of Henry Stommel* (ed. B. A. Warren & C. Wunsch), pp. 396–433. Cambridge, Massachusetts, and London: MIT Press.

Barrick, D. E. & Swift, C. T. 1980 *IEEE J. Ocean Engng* **OE-5**, 74–79.

Born, G. H., Dunne, J. A. & Lame, D. B. 1979 *Science, Wash.* **204**, 1405–1406.

Bracalente, E. M., Boggs, D. H., Grantham, W. L. & Sweet, J. L. 1980 *IEEE J. Ocean Engng* **OE-5**, 145–154.

Brown, G. S. 1978 *IEEE Trans. Antennas Propagation* **AP-26**, 472–482.

Cartwright, D. E. & Alcock, G. A. 1981 In *Oceanography from space* (ed. J. F. R. Gower), pp. 885–895. New York: Plenum.

Chapman, M. E. & Talwani, M. 1979 *J. geophys. Res.* **84**, 3803–3816.

Chelton, D. B., Hussey, K. J. & Parke, M. E. 1981 *Nature, Lond.* **294**, 529.

Cheney, R. E. & Marsh, J. G. 1981 *J. geophys. Res.* 473–483.

Cornuelle, B. A. 1982 *IEEE Trans. Geosci. remote Sens.* (In the press.)

Davies, K., Harmann, G. K. & Leitinger, R. 1977 *J. atmos. terr. Res.* **39**, 571–580.

Deacon, M. 1971 *Scientists and the sea 1650–1900: a study of marine science.* (445 pages.) London and New York: Academic Press.

Douglas, B. C. & Gaborski, P. D. 1979 *J. geophys. Res.* **84**, 4005–4915.

Ekman, V. W. 1953 *Geofys. Publr* **19** (1). (106 and 122 pages.)

European Space Agency 1980 *Study on satellite radar altimetry in climatological and oceanographic research.* (Final Report, prepared by Science Research Council, Rutherford Appleton Laboratories and Natural Environment Research Council, Institute of Oceanographic Sciences, Wormley, Surrey.) (323 pages.)

Fuglister, F. C. & Voorhis, A. D. 1965 *Limnol. Oceanogr. Suppl.*, pp. R115–R134.

Ghil, M. 1980 *Tellus* **32**, 198–206.

Goldhirsh, J. & Rowland, J. R. 1980 *Assessment of atmospheric height uncertainties for high precision satellite altimeter missions to monitor ocean currents.* (Johns Hopkins University Applied Physics Laboratory, JHUV/APL SIR 8OU-018.)

Gordon, A. L. & Baker, T. N. 1980 *J. geophys. Res.* **85**, 502–506.

Gornitz, V., Lebedeff, S. & Hansen, J. 1982 *Science, Wash.* **215**, 1611–1614.

Hansen, J., Johnson, D., Lacis, A., Lebedeff, S., Lee, P., Rind, D. & Russell, G. 1981 *Science, Wash.* **213**, 957–966.

Jekeli, C. & Rapp, R. 1980 *Ohio State Univ. geodet. Sci. Rep.* no. 307.

Johnson, J. W., Williams, L. A. Jr, Bracalente, E. M., Beck, F. B. & Grantham, W. L. 1980 *IEEE J. Ocean Engng* **OE-5**, 138–154.

Jones, W. L., Boggs, D. H., Bracelente, E. M., Brown, R. A., Guymer, T. H., Shelton, D. & Schroeder, L. C. 1981 *Nature, Lond.* **294**, 704–707.

King-Hele, D. 1976 *Science, Wash.* **192**, 1293–1300.

Klepczynski, W. J. (ed.) 1978 *Navigation* (spec. Issue) **25** (2).

Leetmaa, A., McCreary, J. P. Jr & Moore, D. W. 1981 In *Evolution of physical oceanography, scientific surveys in honor of Henry Stommel* (ed. B. A. Warren & C. Wunsch), pp. 184–196. Cambridge, Massachusetts, and London: MIT Press.

Lerch, F., Klosko, S. M., Laubscher, S. M. & Wagner, C. A. 1979 *J. geophys. Res.* **84**, 3897–3916.

Longuet-Higgins, M. S. 1982 *Dyn. Oceans Atmos.* (In the press.)

Marsh, J. G. & Chang, E. S. 1978 *Mar. Geod.* **1**, 253–261.

McWilliams, J. C. & Flierl, G. R. 1976 *Deep Sea Res.* **23**, 285–300.

Mode Group 1978 *Deep Sea Res.* **25**, 859–910.

Moran, J. M. & Rosen, B. R. 1980 In *Radio interferometry techniques for geodesy* (NASA Conference Publication no 2115), pp. 363–376.

Munk W., Worcester, P. & Zachariasen, F. 1981 *J. phys. Oceanogr.* **11**, 442–454.

Munk, W. & Wunsch, C. 1979 *Deep Sea Res.* **26**, 123–161.

Munk, W. & Wunsch, C. 1982*a* *Deep Sea Res.* (In the press.)

Munk, W. & Wunsch, C. 1982*b* (In preparation.)

Needler, G. 1971 *Deep Sea Res.* **18**, 895–903.

Ocean Tomography Group 1982 *Nature, Lond.* (In the press.)

O'Brien, J. J., Busalacchi, A. & Kindle, J. 1980 In *Resource management and environmental uncertainty* (ed. D.M.H. Glantz), pp. 159–212. New York: Wiley.

Pedlosky, J. 1979 *Geophysical fluid dynamics.* (624 pages.) New York: Springer-Verlag.

PHILOSOPHICAL TRANSACTIONS OF THE ROYAL SOCIETY A MATHEMATICAL, PHYSICAL & ENGINEERING SCIENCES

Pillsbury, J. E. 1891 In *Report of the Superintendent of the U.S. Coast And Geodetic Survey showing the Progress of the Work during the Fiscal Year Ending with June 1890*, appendix no. 10, pp. 459–620. Washington.
Reid, J. L. 1981 In *Evolution of physical oceanography, scientific surveys in honor of Henry Stommel* (ed. B. A. Warren & C. Wunsch), pp. 70–111. Cambridge, Massachusetts, and London: MIT Press.
Roemmich, D. & Wunsch, C. 1982 *J. mar. Res.* (In the press.)
Rossby, T. R. 1975 *J. mar. Res.* **33**, 213–222.
Saunders, P. M. 1976 *J. mar. Res.* **24**, 155–160.
Schwiderski, E. W. 1980 *Rev. Geophys. Space Phys.* **18**, 243–268.
Semtner, A. J. & Mintz, Y. 1977 *J. phys. Oceanogr.* **7**, 208–230.
Spiesberger, J. L., Spindel, R. C. & Metzger, K. 1980 *J. acoust. Soc. Am.* **67**, 2011–2017.
Stommel, H. 1965 *The Gulf Stream: a physical and dynamical description*, 2nd edn. (248 pages.) University of California Press.
Stommel, H. & Arons, A. B. 1960 *Deep Sea Res.* **6**, 217–233.
Stommel, H. & Schott, F. 1977 *Deep Sea Res.* **24**, 325–329.
Topex Precision Orbit Determination Group 1980 *A preliminary TOPEX Orbit accuracy analysis.* (*University of Texas at Austin tech. Rep.* no. IASOM TR 80-4.) (50 pages.)
Topex Science Working Group 1981 *Satellite altimetric measurements of the ocean.* (78 pages.) Jet Propulsion Laboratory, Pasadena.
Townsend, W. F. 1980 *IEEE Trans. Ocean Engng* **OE-5**, 80–92.
Walsh, E. J., Uliana, E. A. & Yaplee, B. S. 1978 *Bound. Layer Met.* **13**, 263–276.
Warren, B. A. 1981 In *Evolution of physical oceanography, scientific surveys in honor of Henry Stommel* (ed. B. A. Warren & C. Wunsch), pp. 6–41. Cambridge, Massachusetts, and London: MIT Press.
Welander, P. 1971 *J. mar. Res.* **29**, 60–68.
Worcester, P. 1977 *J. acoust. Soc. Am.* **62**, 895–905.
Wunsch, C. & Minster, J. F. 1982 *J. geophys. Res.* (In the press.)
Wunsch, C. & Gaposchkin, E. M. 1980 *Rev. Geophys. Space Phys.* **18**, 725–745.
Zlotnicki, V. 1982 Ph.D. thesis, Massachusetts Institute of Technology and Woods Hole Oceanographic Institution.
Zlotnicki, V., Parsons, B. & Wunsch, C. 1982 *J. geophys. Res.* **87**, 825–848.

PHILOSOPHICAL TRANSACTIONS OF THE ROYAL SOCIETY A MATHEMATICAL, PHYSICAL & ENGINEERING SCIENCES

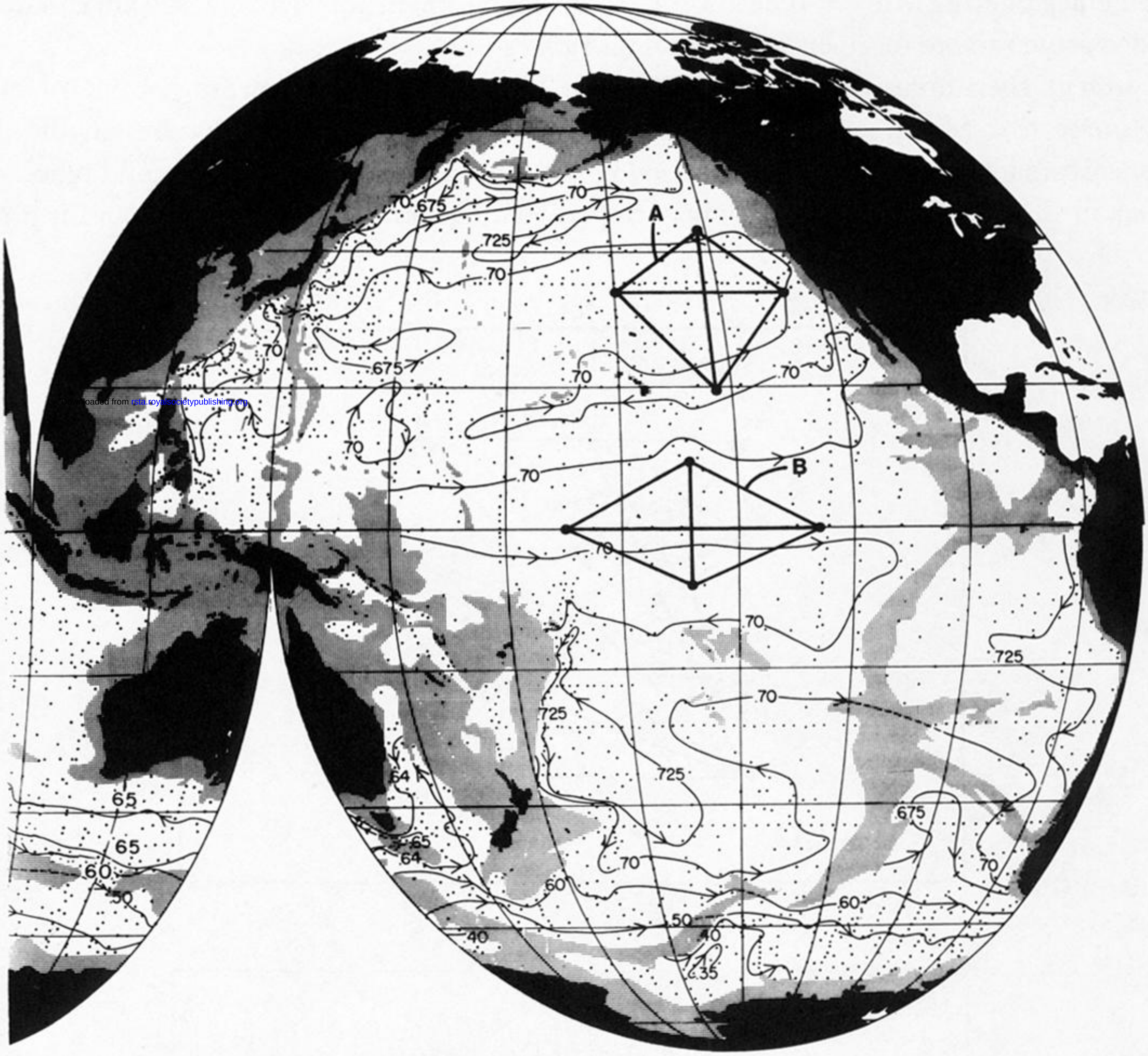

FIGURE 2. Possible subtropical (A) or equatorial (B) arrays in the eastern Pacific, on a 2500 km scale. Co-located sources and receivers permit temperature and velocity determination along six paths. Vorticity can be determined within each of the four sub-triangles, as well as within the entire diamond array. (Chart from Reid (1981).)

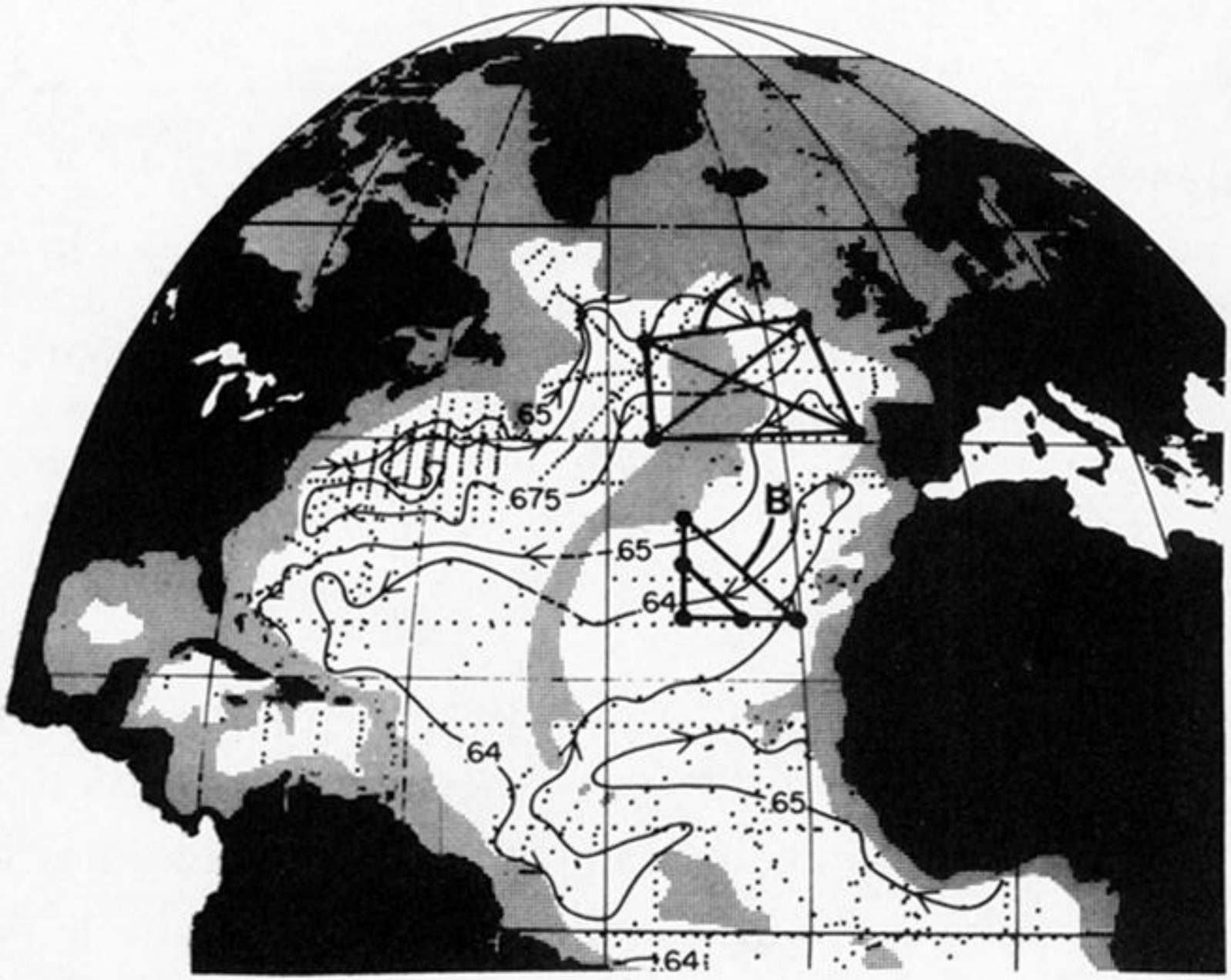

FIGURE 3. (A) Four-point subpolar array in the North Atlantic. (B) A mooring array in the eastern Atlantic basin for studying the vorticity balance (beta spiral).

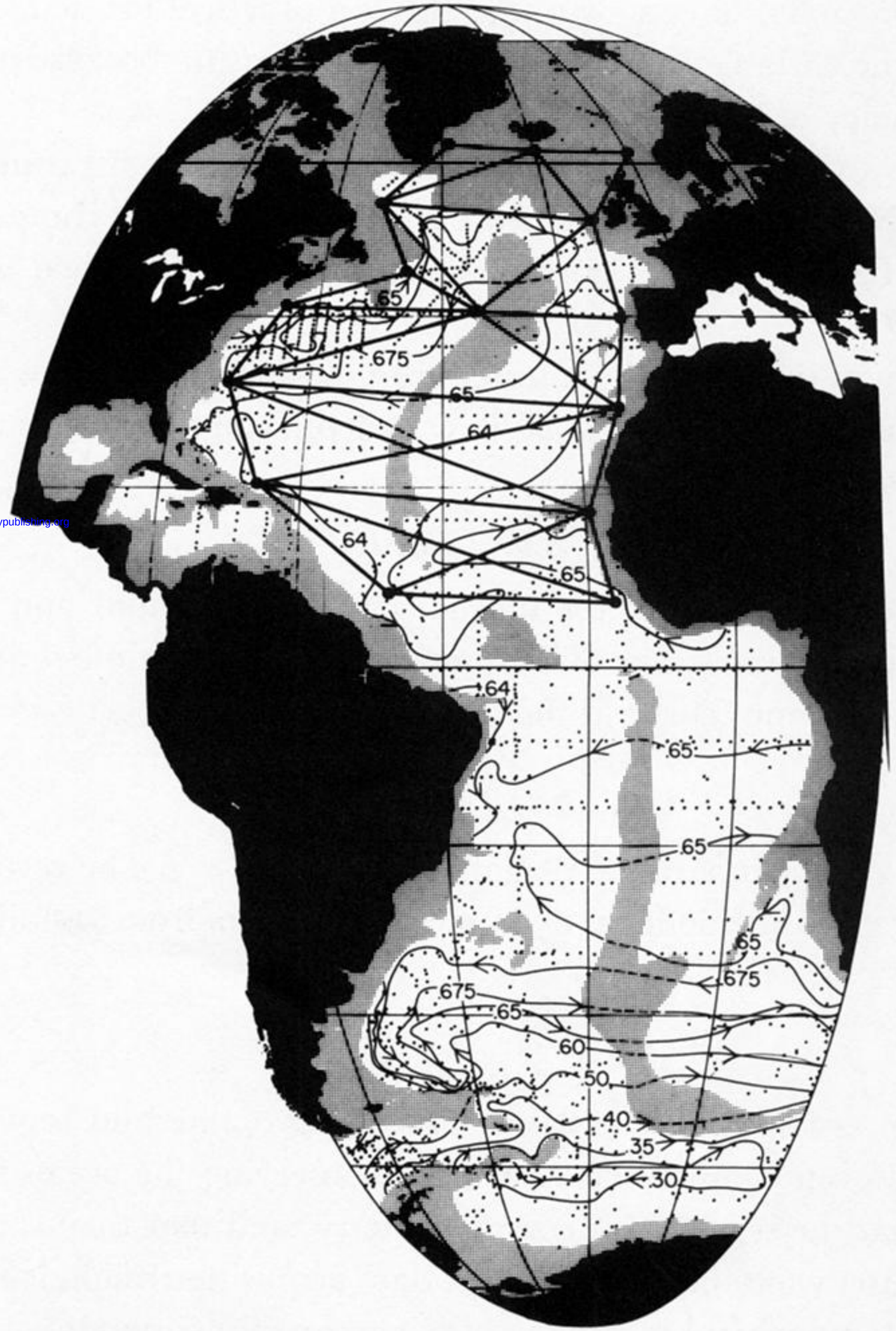

FIGURE 9. A 15 mooring tomographic array in the North Atlantic. Only the nearest-neighbour paths have been drawn. There are a total of 105 paths, and for each of these there are about 10 rays in the vertical plane. Tomography over such large distances requires further engineering developments. Data from this array and from satellite altimetry and scatterometry would be assimilated into a numerical model.

PHILOSOPHICAL TRANSACTIONS OF THE ROYAL SOCIETY A MATHEMATICAL, PHYSICAL & ENGINEERING SCIENCES